



Highly dispersed ultra-fine Ru nanoparticles anchored on nitrogen-doped carbon sheets for efficient hydrogen evolution reaction with a low overpotential

Menghan Gao^a, Zhihong Wang^a, Shichao Sun^a, Deli Jiang^a, Wenxian Wei^b, Min Chen^{a,*}

^a School of Chemistry and Chemical Engineering, Jiangsu University, 301Xuefu Road, Zhenjiang 212013, China

^b Testing center, Yangzhou University, 48 East Wenhui Road, Yangzhou 225009, China



ARTICLE INFO

Article history:

Received 19 September 2020

Received in revised form 29 October 2020

Accepted 30 November 2020

Available online 2 December 2020

Keywords:

Electrocatalysis

Hydrogen evolution reaction

Ru nanoparticles

Nitrogen-doped carbon

Synergistic effect

ABSTRACT

Development of highly efficient and cost-effective hydrogen evolution reaction (HER) electrocatalyst that rivals benchmark Pt is highly desirable but challenging. In this work, the integration of uniformly dispersed ultra-fine Ru nanoparticles with the nitrogen-doped carbon sheets (NCs) is reported as an efficient electrocatalyst. The Ru/NCs composite catalyst possesses abundant catalytic activity sites, and the synergy effect between Ru and NCs can modulate the electronic structure and adsorption of reaction intermediate to enhance the HER activity. Remarkably, the optimal 20% Ru/NCs catalyst delivers an overpotential of as low as 13 mV at the current density of 10 mA cm⁻² and with a Tafel slope of 31.8 mV dec⁻¹, which is superior to most of recently reported Ru-based electrocatalysts and even, superior to the state of the art Pt/C catalyst. This work provides an effective strategy for the development of ultra-efficient electrocatalyst for the water splitting in alkaline condition.

© 2020 Published by Elsevier B.V.

1. Introduction

Fuel depletion has led to a rapid increase in the demand for sustainable and clean energy. Driven by this, hydrogen, with the advantages of high gravimetric energy density, non-pollution and earth-abundance has evoked extensive attention [1–4]. Electrochemical water splitting provides an industrial-scale method for producing large quantities of pure hydrogen [5]. One of the key to develop electrochemical water splitting is to exploit a high efficient, long-term stable and low-cost electrocatalyst for HER. Up to now, Pt-based electrocatalysts are at the forefront of HER catalysts research field for their unparalleled activity [6–8]. However, the scarcity of Pt leads to an exorbitant prices, which vastly limits the practical application of it [9,10]. Transition metals-based electrocatalysts have been extensively explored as potential alternatives to Pt-based electrocatalysts in the past few decades [11–13]. But the catalytic activity of most of transition metal-based is still unsatisfactory to meet the demand, as the adsorption energy of H* on the surface of transition metal-based catalysts is generally improper [14–17]. Therefore, development of high performance and relatively low-cost

electrocatalyst that exceeds the Pt-based catalysts is still highly desirable but remains great challenging.

An ideal HER electrocatalysts must follow the Sabatier principle, that is, the adsorption energy of H* on the surface of electrocatalysts should not be too high, nor too low [18]. Pt-group metals (M) such as Ru, Rh and Ir can form M-H* bond with moderate energy, which is conducive to regulate the adsorption and desorption of H* and effectively decrease the overpotential of HER [19,20]. Among them, Ru holds the lowest price and has received great attention due to its superior HER performance in alkaline solution. Construction of Ru-based composite catalyst is an effective strategy to further enhance the HER activity, which can be attributed to the synergistic effect of the different component to optimize the adsorption energy of the catalysts, maximize the number of active site and enhance the stability of the catalysts. For example, Li and co-workers developed the electrocatalyst of nano-Ru decorated cobalt carbonate hydroxides nanowires on carbon fiber (CF@Ru-CoCH NWs) and the electrocatalyst displayed a low HER overpotential (66 mV@10 mA cm⁻²) and Tafel slope (65 mV dec⁻¹) [21]. Recently, Qiao et al. prepared Ru/C₃N₄/C hybrid electrocatalyst and obtained a much lower HER overpotential (79 mV@10 mA cm⁻²) compared to the Ru/C counterpart [22]. In another limited example, Baek et al. have demonstrated that the integration of Ru nanoparticles with nitrogenated holey two-dimensional carbon could synergistically enhance the HER activity,

* Corresponding author.

E-mail address: chenmin3226@sina.com (M. Chen).

and a very low HER overpotential (17 mV @ 10 mA cm⁻²) in alkaline solution was achieved [23]. However, the report on the Ru-based composite catalyst with high HER activity superior to the benchmark Pt catalyst remains rare. Therefore, it is urgent but challenging to design novel Pt-free Ru-based composite catalyst with high-performance HER activity.

Inspired by above reasons, in this work, we reported an ultra-efficient HER catalyst, which integrated uniformly dispersed ultra-fine Ru nanoparticles with the nitrogen-doped carbon sheets. As carrier, 2D NCs not only provide the localized site for the growth of Ru nanoparticles to prevent the agglomeration of particles and maximizes the exposure of active sites, but also improve the catalytic activity and stability of Ru/NCs. Remarkably, the optimal 20% Ru/NCs catalyst delivers an overpotential as low as 13 mV at the current density of 10 mA cm⁻² and with a Tafel slope of 31.8 mV dec⁻¹, which is superior to most of recently reported Ru-based electrocatalysts and even, superior to benchmark Pt/C catalyst. Given ultrahigh catalytic performance and relatively low-cost, Ru/NCs is expected an alternative to the Pt/C electrocatalyst to apply in the practical water splitting.

2. Experimental

2.1. Synthesis of electrocatalysts

2.1.1. Synthesis of NCs

The NCs sample was fabricated according to previous report [24]. Firstly, 0.1896 g of dopamine hydrochloride and 1.892 g of FeCl₃·6H₂O were placed in a mortar and ground sufficiently to obtain the complex produce, until the product became a flowing black liquid. Secondly, the liquid was directly transferred into a tube furnace. The temperature of tube furnace was raised to 700 °C with the rate of 5 °C min⁻¹ under Ar atmosphere and the reaction was lasted for 2 h. Finally, the resulting product was cleaned with 0.5 M H₂SO₄ to removed impurities during continuous stirring, and then washed with water and dried to obtain the NCs. As a comparison, nitrogen-doped carbon bulk material (denoted as NCb) was prepared by direct calcination of dopamine hydrochloride without adding FeCl₃·6H₂O as template.

2.1.2. Synthesis of Ru/NCs

NCs and RuCl₃ were dispersed in 100 mL of ethylene glycol with the mass ratio of NCs and RuCl₃ of 80 mg: 40 mg. Then, the mixture solution was reflowed in an oil bath at the temperature of 190 °C for 30 min. After centrifugation, several times washes with DI water and drying, the final catalyst was obtained. In the end, the catalyst was named 20% Ru/NCs. In addition, Ru/NCs with other mass percentage were received by changing the mass ratio of NCs and RuCl₃. In the above process, 20% Ru/NCb or pure Ru catalyst can be obtain if NCb was used instead of NCs or without the addition of NCs.

2.2. Characterizations

Raman scattering characterization was recorded on a Renishaw InVia Micro-Raman system with excitation wavelength of 532 nm. X-ray diffraction (XRD) analysis was performed on a Bruker D8 Advance X-ray diffractometer. Transmission electron microscopy (TEM) and high-resolution TEM (HRTEM) measurements were conducted on Tecnai 12 and Tecnai G2 F30 respectively to reveal the morphology of the samples. The X-ray photoelectron spectra (XPS) were determined by an ESCA PHI500 spectrometer. The nitrogen adsorption/desorption measurements were used to analyze Brunauer-Emmett-Teller (BET) surface area of the as prepared products on a surface area analyzer (Micromeritics Instrument Corporation, USA). Inductively coupled plasma-atomic emission spectroscopy (ICP-AES) were carried out on an Varian VISTA-MPX instrument.

2.3. Electrochemical measurements

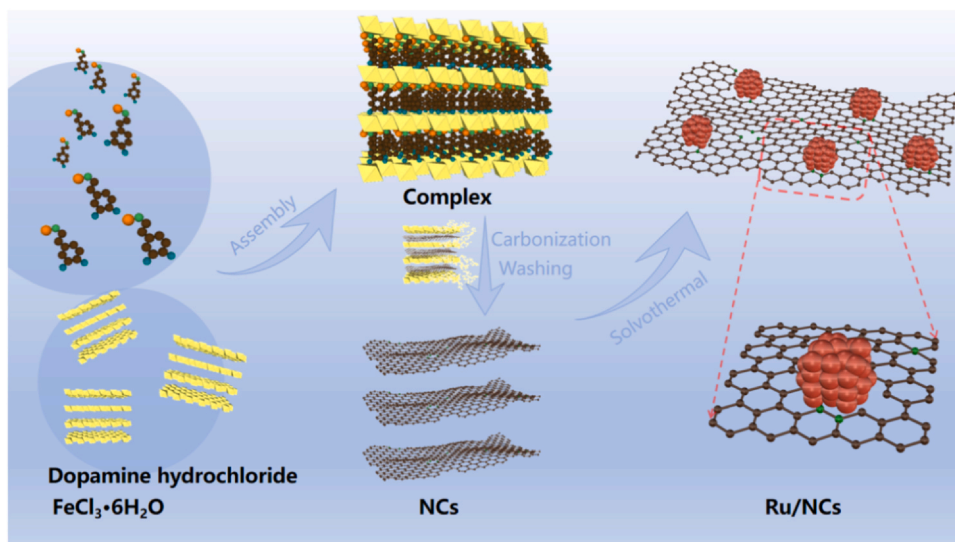
To prepare the working electrode, the electrocatalyst (5 mg), ethanol (1 mL) and Nafion (40 μL) were mixed and dispersed evenly by ultrasonication for 30 min. Then, 5 μL of the suspension was attached to a cleaned glassy carbon electrode (GCE, 3 mm diameter, loading amount of 0.34 mg cm⁻²). Electrochemical measurements were performed on a CHI-760E electrochemical workstation with a three-electrode configuration. In 1 M KOH (pH = 13.6) electrolyte, a modified GCE, Ag/AgCl electrode and graphite rod were respectively used as working electrode, reference electrode and counter electrode. Potentials were converted to hydrogen electrodes (RHE) by the equation of $E_{RHE} = E_{Ag/AgCl} + 0.197V + 0.059 \times pH$. Linear sweep voltammetry (LSV) curves at a scan rate of 5 mV s⁻¹ were selected to evaluate the electrocatalytic activities of the samples. The equation of $\eta = b \log j + a$ provided a reference for the calculation of Tafel plots, where j , b and a represent the current density (mA cm⁻²), Tafel plot and intercept relative to the exchange current density, respectively. Mass activity (A g⁻¹) were calculated from the mass loading m (0.34 mg cm⁻²) and the current density j at overpotential at -0.07 V, according to the formula of $Mass\ activity = j/m$. The electrochemical active surface area (ECSA) can be estimated by the double-layer capacitance (C_{dl}), which obtained from the formula of $C_{dl} = I/\nu$, where I on the behalf of the charging current (mA cm⁻²) and ν refer the scan rate (mV s⁻¹). Electrochemical impedance spectroscopy (EIS) was measured at a frequency range of 0.01–100000 Hz. Successive CV and multistep chronopotential method were adopted to test the stability of 20% Ru/NCs. The Faradaic efficiency of electrocatalyst was calculated according to the equation of $Faradaic\ efficiency = (2 \times F \times NH_2)/(I \times t)$, where the value of F is 96485 C mol⁻¹ and N_{H_2} , I and t are the mole of the generated H₂, constant reduction current and time for constant reduction current, respectively.

3. Results and discussion

The experiment involves the preparation of two-dimensional NCs by salt-templating method and followed by the fabrication of Ru nanoparticles through mild solvothermal method. The relevant processes are shown in Scheme 1. Briefly, 2D NCs with large specific area was obtained after complexation, calcination and washing, with dopamine hydrochloride as raw material and FeCl₃·6H₂O as template. Then, 2D NCs was used as substrates to provide anchoring site for the growth of Ru nanoparticles.

Morphology characterization was carried out by TEM and HRTEM. The TEM images of 20% Ru/NCs are shown in Fig. 1a–c. Figs. 1a and S1a and b prove that the NCs presents a large 2D flake structure, while Fig. 1b and c reveals a good dispersity of Ru nanoparticles on NCs. Meanwhile, the HRTEM image (Fig. 1d) manifests the size distribution of Ru nanoparticles is about 3 nm. However, this good dispersion disappears in pure Ru (Fig. S1c and d) and 20% Ru/NCb electrocatalysts (Fig. S1e and f) and replaced by the morphology of large particles with agglomeration. Nanoparticles with smaller size are conducive to the exposure of active sites to improve catalytic efficiency [25]. Therefore, we consider that NCs play a significance role in the dispersion of Ru, and we can also speculate that the 20% Ru/NCs may have better catalytic activity than pure Ru and 20% Ru/NCb due to the exposure of more active sites. In Fig. 1e, the lattice distance of 0.234, 0.214 and 0.208 nm match well with the (100), (002) and (101) planes of Ru (PDF card #06-0663). Similarly, the obvious characteristic ring corresponding to (101) plane is also shown in the selected area electron diffraction (SEAD) pattern (Fig. 1f), accompanied by the weaker spot of the (100), (110) and (112). The HAADF-STEM images and elemental mappings (Fig. 1g) confirm the uniform doping of N in carbon and the well dispersion of Ru on NCs.

The graphitization degree of NCs and the crystalline phase of Ru/NCs were analyzed by Raman spectroscopy (Fig. 2a) and XRD (Figs. 2b and S2a). In Raman spectra, NCs has two distinct peaks near 1367 and 1580 cm⁻¹, belonging to D and G band respectively, where



Scheme 1. Schematic presentation of synthesis of the Ru/NCs composite.

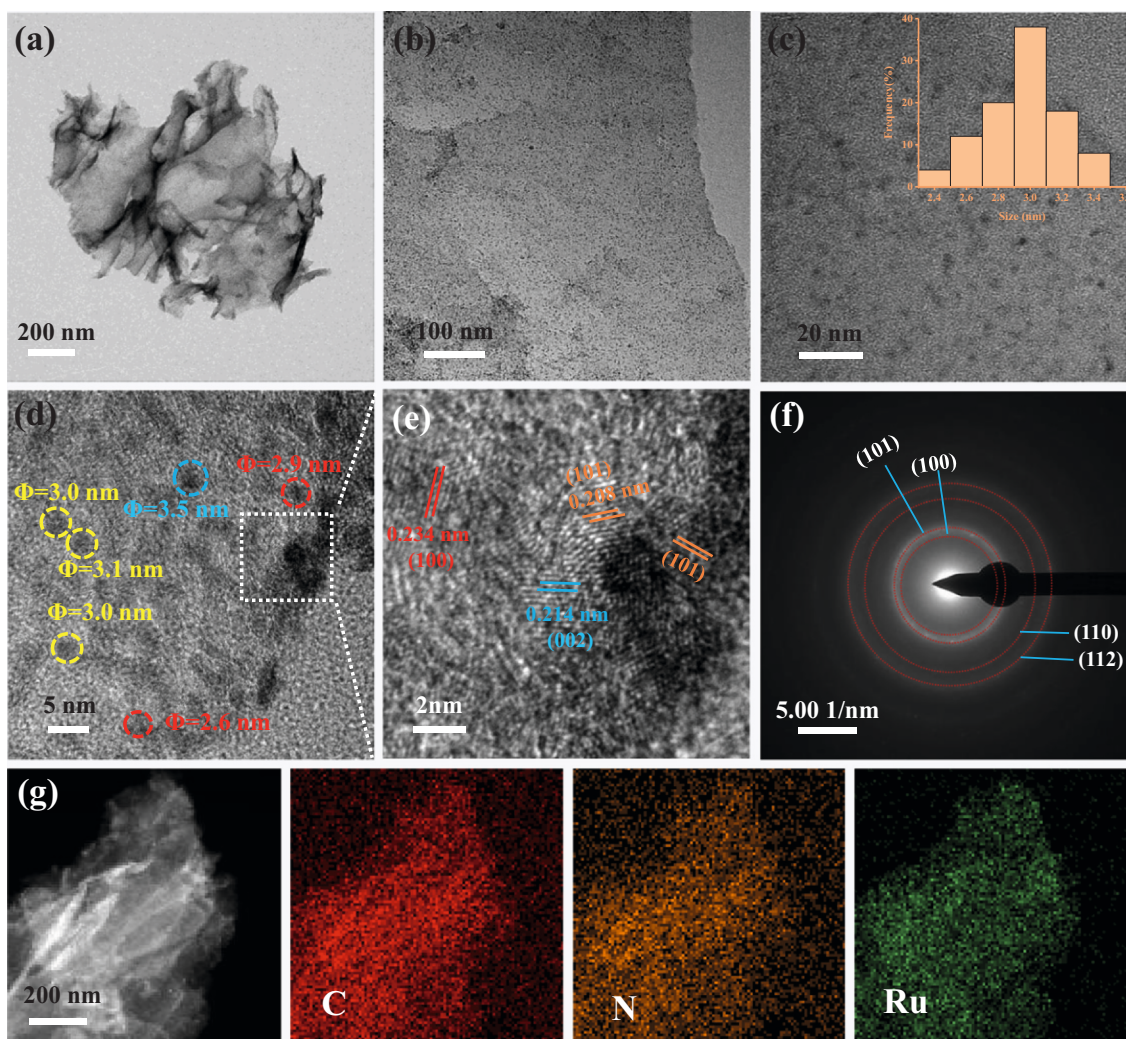


Fig. 1. Structure characterization. (a–c) TEM images, (d and e) HRTEM images, (f) SAED pattern, (g) HAADF-STEM image and corresponding elemental mappings of 20% Ru/NCs.

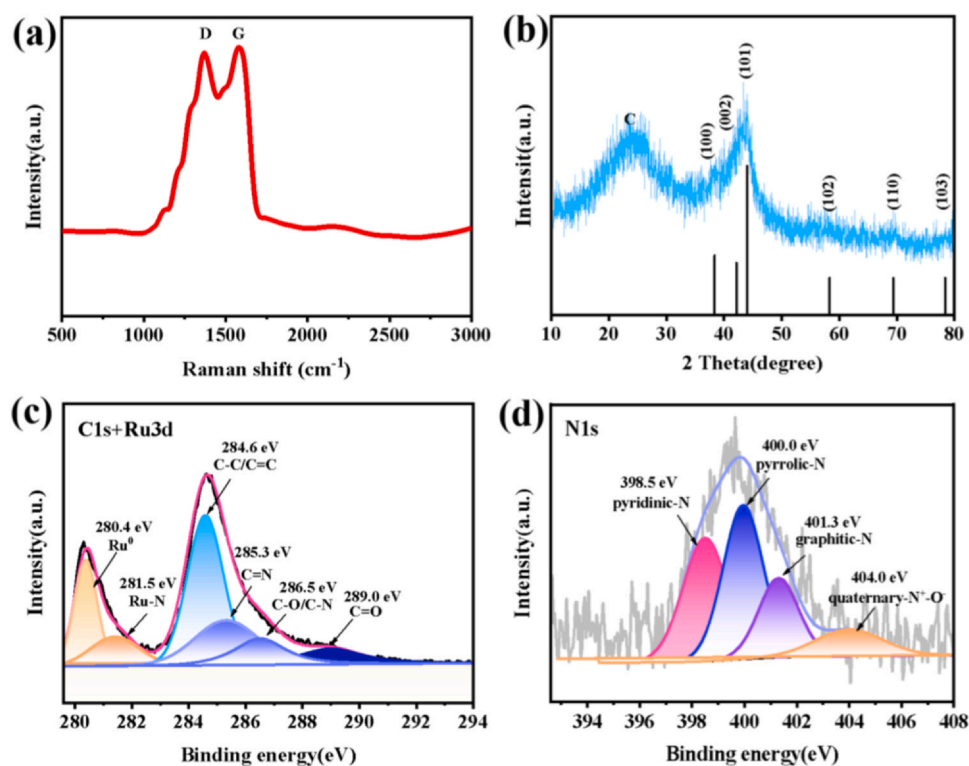


Fig. 2. (a) Raman spectra of NCs. (b) XRD pattern of 20% Ru/NCs. High-resolution XPS spectra of (c) C 1s+Ru 3d, (d) N 1s.

the D band reflects the sp^3 defect site and the G band represents the in-plane stretch vibration of sp^2 band pairs [26]. The intensity ratio of D band to G band is 0.91, indicating the existence of many defects in NCs caused by N doping [27,28]. This nitrogen-doped C will affect the nucleation and growth kinetics of particles catalyst, resulting in smaller particle size and more uniform dispersion, which ultimately change the catalytic efficiency [29]. Furthermore, no obvious 2D band peak was observed, which demonstrate that there is no pronounced graphitic stacking in NCs. Subsequently, the carbon peak (the (002) plane) of NCs was found at 26.4° in XRD patterns [30], while the peaks located at 38.4° , 42.2° , 44.0° , 58.3° , 69.4° and 78.4° can be indexed to (100), (002), (101), (102), (110) and (103) plane of Ru (PDF card #06-0663). The above results prove the high graphitization of NCs and good crystallinity of Ru nanoparticles.

XPS characterization was used to analyze chemical valence states of the electrocatalyst. In the spectrum of C 1s and Ru 3d (Fig. 2c), the C1s peak are well fitted with four peaks at 284.6, 285.3, 286.5 and 289.0 eV, ascribing to the existent of C-C/C=C, C=N, C-N/C-O and C=O, and the relatively strong intensity of C=N portends the relatively high N doping [31]. Two peaks located at 280.4 and 281.5 eV are attributed to Ru^0 and Ru-N coordination, respectively [32]. For the N 1s (Fig. 2d), the binding energy at 398.5, 400.0, 401.3 and 404.0 eV are corresponding to pyridinic-N, pyrrolic-N, graphitic-N and quaternary-N $^+$ -O $^-$, respectively [31]. ICP-AES analysis shows that the mass contain of Ru is around 20% for 20% Ru/NCs. It can be inferred from the above results that the existence of N has affected the electronic structure of Ru, which may be more beneficial for HER reaction [33].

For powdery electrocatalyst, the influence of surface area on electrocatalytic performance should not be underestimated. Therefore, N_2 -adsorption-desorption measurement was performed to study the surface area and pore distribution of electrocatalysts. As shown in Fig. S2b, the type IV isotherm suggests the presence of mesopores. The Brunauer-Emmett-Teller surface area of NCs, 20% Ru/NCs and 20% Ru/NCb were 1312, 770 and $54 \text{ m}^2 \text{ g}^{-1}$, respectively. High BET surface area of the 20% Ru/NCs could provide a large number of active site, which is favorable for the catalytic activity.

The HER activity of as-prepared electrocatalysts were tested in 1.0 M KOH. Based on the polarization curves in Fig. 3a, the overpotential comparison diagram (Fig. 3b) of catalysts at current density of 10 and 100 mA cm^{-2} is given. First, it is clearly observed that the NCs have low catalytic activity in the measurement. Then, the 20% Ru/NCs shows the lowest overpotential (13 mV at 10 mA cm^{-2} and 133 mV at 100 mA cm^{-2}) than 20% Ru/NCb (89 mV at 10 mA cm^{-2} and 387 mV at 100 mA cm^{-2}) and pure Ru electrocatalysts (26 mV at 10 mA cm^{-2} and 181 mV at 100 mA cm^{-2}). Combining the above overpotential data with the results of TEM and BET, it can be demonstrated that the combination of ultra-small Ru nanoparticles and NCs is beneficial to HER activity. Finally, the HER performance of 20% Ru/NCs is found to be superior to the commercial 20% Pt/C (17 mV at 10 mA cm^{-2} and 167 mV at 100 mA cm^{-2}). Which is mainly attributed to the interaction between metal particles and the carbon substrates, which optimizes the electronic structure of the metal particles to make catalyst show improved HER activity. This superior electrochemical activity to the commercial Pt/C confirms our prediction of XPS result. Furthermore, the polarization curves of Ru/NCs with other mass percentages of Ru are shown in Fig. S3a. When the Ru content increased from 5% to 10%, 20% and 30%, the corresponding overpotential at the current density of 10 mA cm^{-2} were 22, 19, 13 and 13 mV, which were all lower than the 26 mV of pure Ru, proving that the more Ru dispersed in NCs, the more favorable to catalysis, but excess Ru will also hinder the further enhancement of performance. Moreover, to further explore the catalytic activity of 20% Ru/NCs, HER performance in 0.1 M and 30 wt% KOH and near-neutral BPS (1 M, pH=6.9) were also measured (Fig. S3b-d). As we can see, 20% Ru/NCs exhibits higher performance than 20% Pt/C in 0.1 M and 30 wt% KOH, while the overpotential is lower than 20% Pt/C in 1 M PBS, indicating that 20% Ru/NCs work better in alkaline electrolyte.

In order to probe the HER kinetics, the Tafel plots of the electrocatalyst were collected. As shown in Fig. 3c, the Tafel slope of 31.8 mV dec^{-1} for 20% Ru/NCs, which is smaller than that of $186.0 \text{ mV dec}^{-1}$ for 20% Ru/NCb and of 55.2 mV dec^{-1} for Ru. Meanwhile, the

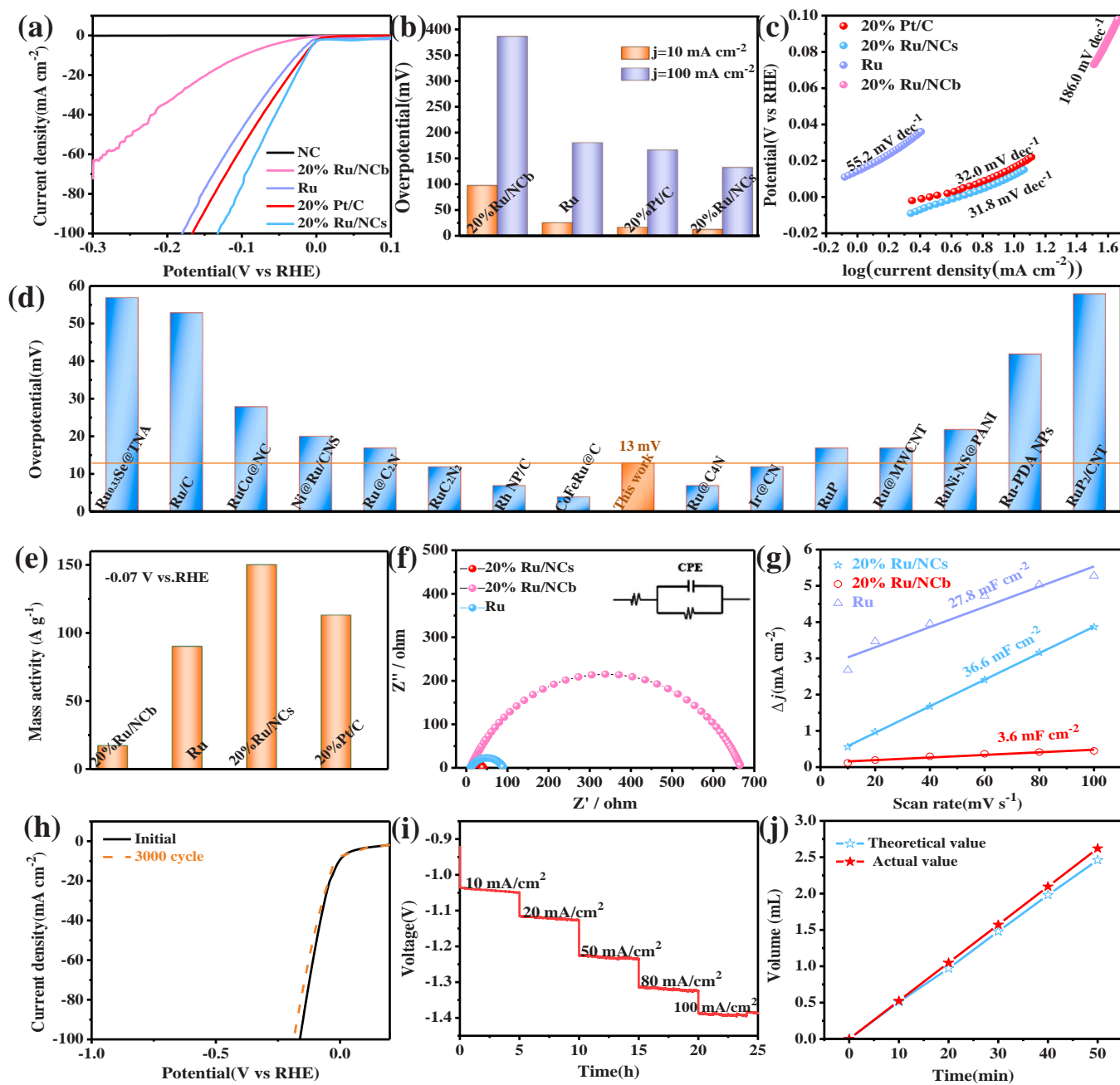


Fig. 3. (a) Polarization curves, (b) overpotential at 10 and 100 mA cm⁻² and, (c) Tafel slopes of different catalysts. (d) Comparisons of the overpotential at the current density of 10 mA cm⁻² for Ru/NCS with recently reported precious metal-based catalysts. (e) Mass activity at -0.07 V vs. RHE of different catalysts. (f) Electrochemical impedance and, (g) Calculated electrochemical double-layer capacitance for 20% Ru/NCb, Ru and 20% Ru/NCS electrocatalyst. (h) LSV curves before and after 3000 cycles, (i) the multistep chronopotentiometric curve and, (j) HER efficiency of 20% Ru/NCS electrocatalyst.

approximate Tafel slope with 20% Pt/C (32.0 mV dec⁻¹) indicates that the rate-controlling step of 20% Ru/NCS is Tafel-Volmer mechanism. Compared the above electrochemical performance with recently reported noble-metal-based catalysts (Fig. 3d and Table S1), our catalyst performs competitive activity [20–22,31–45]. To define the catalytic properties, mass activity was calculated (Fig. 3e). At an overpotential of -0.07 V vs RHE, the 20% Ru/NCS presents a mass activity of 150.5 mA g⁻¹, which is 1.33, 1.66 and 8.55 folds to that of the 20% Pt/C, Ru and 20% Ru/NCb, respectively, proving the excellent catalytic performance of 20% Ru/NCS.

To further get insight into the excellent activity of 20% Ru/NCS, electrochemical impedance spectroscopies (ESI) and electrochemical active areas (ECSA) were measured. One can see from Fig. 3f, at a potential of -1.04 V vs Ag/AgCl, the diameter of the semicircle of 20%

Ru/NCS is much smaller than Ru and 20% Ru/NCb, portending that the synergy between NCS and Ru results in the lowest contact and charge-transfer impedance of 20% Ru/NCS. According to CV curves at the scan rates of 10, 20, 40, 60, 80 and 100 mV within potential range of 0.052–0.152 V (Fig. S4a–c), C_{dl} were fitted in Fig. 3g to evaluate the ECSA. It was calculated that the ECSA of 20% Ru/NCS, Ru and 20% Ru/NCb were 36.6, 27.8 and 3.6 mF cm⁻², respectively. Benefiting from the large specific surface area of NCS, 20% Ru/NCS exposed more activate sites, which could enhance the HER activity.

The stability of 20% Ru/NCS was proved by CV and multistep chronopotentiometric method. Fig. 3h shows two similar LSV curves of 20% Ru/NCS before and after 3000 cycles, revealing that 20% Ru/NCS possess good stability. In addition, the multistep chronopotentiometric curve in Fig. 3i further confirm the long-term durability of 20% Ru/

NCs in 1 M KOH. The electrocatalyst was tested for 5 h respectively at the current density of 10, 20, 50, 80 and 100 mA cm⁻², and the curves at each step were relatively stable. The good stability is not only attributed to the good corrosion resistance provided by carbon material, but also since the doping of N enhances the chemical bond between the catalyst and the substrate, resulting in increased stability. TEM images in S5a demonstrate that the morphology of the post catalyst changed little after long-term durability. XPS spectra of C 1s+Ru 3d of post catalyst is shown in Fig. S5b, indicating the formation of RuO₂, which is the main reason for the declining performance of the 20% Ru/NCs. In the end, the Faradaic efficiency of 20% Ru/NCs for HER is determined to be 94.4% from theoretical value and detected hydrogen amounts (Fig. 3j), which confirms the practicability of our electrocatalyst.

4. Conclusions

In summary, we have developed a novel Ru/NCs electrocatalyst by early carbonization and subsequent solvothermal reaction. The carbon sheets prepared by the template method provide a large specific surface area which are conducive to the anchoring of Ru. The resulting Ru nanoparticles show uniform dispersion with an average diameter of 3 nm. Remarkably, the optimal 20% Ru/NCs catalyst delivers an overpotential of as low as 13 mV at the current density of 10 mA cm⁻² and with a Tafel slope of 31.8 mV dec⁻¹, which is superior to most of recently reported Ru-based electrocatalysts and even, superior to the state of the art Pt/C catalyst. In view of ultrahigh catalytic performance and relatively low-cost, Ru/NCs is considered to be a substitute for Pt/C electrocatalyst to apply in the practical water splitting.

CRedit authorship contribution statement

Menghan Gao: Conceptualization, Writing - original draft preparation. **Zhihong Wang:** Data curation, Investigation. **Shichao Sun:** Visualization, Investigation. **Delijiang:** Writing - reviewing, editing. **Wenxian Wei:** Methodology, **Min Chen:** Validation.

Declaration of Competing Interest

There is no conflict of interest.

Acknowledgements

This work was supported by the financial supports of National Natural Science Foundation of China (22075111 and 21878130) and China Postdoctoral Science Foundation (2018M642180).

Appendix A. Supporting information

Supplementary data associated with this article can be found in the online version at doi:10.1016/j.jallcom.2020.158174.

References

- [1] X.Q. Du, Z. Yang, Y. Li, Y.Q. Gong, M. Zhao, Controlled synthesis of Ni(OH)₂/Ni₃S₂ hybrid nanosheet arrays as highly active and stable electrocatalysts for water splitting, *J. Mater. Chem. A* 6 (2018) 6938–6946.
- [2] D.L. Jiang, Y. Xu, R. Yang, D. Li, S.C. Meng, M. Chen, CoP₃/CoMoP heterogeneous nanosheet arrays as robust electrocatalyst for pH-universal hydrogen evolution reaction, *ACS Sustain. Chem. Eng.* 7 (2019) 9309–9317.
- [3] T. Wang, X.J. Wang, Y. Liu, J. Zheng, X.G. Li, A highly efficient and stable biphasic nanocrystalline Ni-Mo-N catalyst for hydrogen evolution in both acidic and alkaline electrolytes, *Nano Energy* 22 (2016) 111–119.
- [4] R. Yang, Y.M. Zhou, Y.Y. Xing, D. Li, D.L. Jiang, M. Chen, W.D. Shi, S.Q. Yuan, Synergistic coupling of CoFe-LDH arrays with NiFe-LDH nanosheet for highly efficient overall water splitting in alkaline media, *Appl. Catal. B-Environ.* 253 (2019) 131–139.
- [5] X.Q. Du, G.Y. Ma, X.S. Zhang, Experimental and theoretical understanding on electrochemical activation processes of nickel selenide for excellent water-splitting

- performance: comparing the electrochemical performances with M–NiSe (M= Co, Cu, and V), *ACS Sustain. Chem. Eng.* 7 (2019) 19257–19267.
- [6] T.T. Sun, N.N. Shan, L.B. Xu, J.F. Chen, A.A. Zakhidov, R.H. Baughman, General synthesis of 3D ordered macro/mesoporous materials by templating mesoporous silica confined in opals, *Chem. Mater.* 30 (2018) 1617–1624.
- [7] Z.P. Xiang, H.Q. Deng, P. Peljo, Z.Y. Fu, S.L. Wang, D. Mandler, G.Q. Sun, Z.X. Liang, Electrochemical dynamics of a single platinum nanoparticle collision event for the hydrogen evolution reaction, *Angew. Chem. Int. Ed.* 130 (2018) 3522–3526.
- [8] Z.J. Chen, G.X. Cao, L.Y. Gan, H. Dai, N. Xu, M.J. Zang, H.B. Dai, H. Wu, P. Wang, Highly dispersed platinum on honeycomb-like NiO@Ni film as a synergistic electrocatalyst for the hydrogen evolution reaction, *ACS Catal.* 8 (2018) 8866–8872.
- [9] M.H. Sun, J.P. Ji, M.Y. Hu, M.Y. Weng, Y.P. Zhang, H.S. Yu, J.J. Tang, J.C. Zheng, Z. Jiang, F. Pan, C.D. Liang, Z. Lin, Overwhelming the performance of single atoms with atomic clusters for platinum-catalyzed hydrogen evolution, *ACS Catal.* 9 (2019) 8213–8223.
- [10] Z.P. Zhao, H.T. Liu, W.P. Gao, W. Xue, Z.Y. Liu, J. Huang, X.P. Pan, Y. Huang, Surface-engineered PtNi-O nanostructure with record-high performance for electrocatalytic hydrogen evolution reaction, *J. Am. Chem. Soc.* 140 (2018) 9046–9050.
- [11] J.W. Huang, Y. Su, Y.D. Zhang, W.Q. Wu, C.Y. Wu, Y.H. Sun, R.F. Lu, G.F. Zou, Y.R. Li, J. Xiong, FeO_x/FeP hybrid nanorods neutral hydrogen evolution electrocatalysis: insight into interface, *J. Mater. Chem. A* 6 (2018) 9467–9472.
- [12] D.L. Jiang, W.X. Ma, Y.M. Zhou, Y.Y. Xing, B. Quan, D. Li, Coupling Co₂P and CoP nanoparticles with copper ions incorporated Co₉S₈ nanowire arrays for synergistically boosting hydrogen evolution reaction electrocatalysis, *J. Colloid Interface Sci.* 550 (2019) 10–16.
- [13] X.Q. Du, H. Su, X.S. Zhang, Metal-organic framework-derived M (M= Fe, Ni, Zn and Mo) doped Co₉S₈ nanoarrays as efficient electrocatalyst for water splitting: the combination of theoretical calculation and experiment, *J. Catal.* 383 (2020) 103–116.
- [14] L. Yang, H. Zhou, X. Qin, X.D. Guo, G.W. Cui, A.M. Asiri, X.P. Sun, Cathodic electrochemical activation of Co₃O₄ nanoarrays: a smart strategy to significantly boost the hydrogen evolution activity, *Chem. Commun.* 54 (2018) 2150–2153.
- [15] Y.J. Guo, D. Guo, F. Ye, K. Wang, Z.Q. Shi, X.J. Chen, C. Zhao, Self-supported NiSe₂ nanowire arrays on carbon fiber paper as efficient and stable electrode for hydrogen evolution reaction, *ACS Sustain. Chem. Eng.* 6 (2018) 11884–11891.
- [16] C. Wu, J.H. Li, Unique hierarchical Mo₂C/C nanosheet hybrids as active electrocatalyst for hydrogen evolution reaction, *ACS Appl. Mater. Interfaces* 9 (2017) 41314–41322.
- [17] J.D. Benck, T.R. Hellstern, J. Kibsgaard, P. Chakhranont, T.F. Jaramillo, Catalyzing the hydrogen evolution reaction (HER) with molybdenum sulfide nanomaterials, *ACS Catal.* 4 (2014) 3957–3971.
- [18] A.B. Laursen, S. Kegnaes, S. Dahl S, I. Chorkendorff, Molybdenum sulfides-efficient and viable materials for electro- and photoelectrocatalytic hydrogen evolution, *Energy Environ. Sci.* 5 (2012) 5577–5591.
- [19] M. Hu, M. Ming, C.L. Xu, Y. Wang, D.J. Gao, J. Bi, G.Y. Fan, Towards high-efficiency hydrogen production through in situ formation of well-dispersed rhodium nanoclusters, *ChemSusChem* 11 (2018) 3253–3258.
- [20] H. Wang, M. Ming, M. Hu, C.L. Xu, Y. Wang, Y. Zhang, D.J. Gao, J. Bi, G.Y. Fan, H.J. Song, Size and electronic modulation of iridium nanoparticles on nitrogen-functionalized carbon toward advanced electrocatalysts for alkaline water splitting, *ACS Appl. Mater. Interfaces* 10 (2018) 22340–22347.
- [21] J.C. Li, Q.W. Zhou, Z.H. Shen, S.W. Li, J. Pu, C.L. Zhong, M.Q. Cao, H.G. Zhang, Y.Y. Wang, H.X. Ma, Synergistic effect of ultrafine nano-Ru decorated cobalt carbonate hydroxides nanowires for accelerated alkaline hydrogen evolution reaction, *Electrochim. Acta* 331 (2020) 135367.
- [22] Y. Zheng, Y. Jiao, Y.H. Zhu, L.H. Li, Y. Han, Y. Chen, M. Jaroniec, S.Z. Qiao, High electrocatalytic hydrogen evolution activity of an anomalous ruthenium catalyst, *J. Am. Chem. Soc.* 138 (2016) 16174–16181.
- [23] J. Mahmood, J. F. Li, S.M. Jung, M.S. Okyay, I. Ahmad, S.J. Kim, N.J. Park, H.Y. Jeong, J.B. Beak, An efficient and pH-universal ruthenium-based catalyst for the hydrogen evolution reaction, *Nat. Nanotechnol.* 12 (2017) 441–446.
- [24] S. Li, C. Cheng, H.W. Liang, X.L. Feng, A. Thomas, 2D porous carbons prepared from layered organic-inorganic hybrids and their use as oxygen-reduction electrocatalysts, *Adv. Mater.* 29 (2017) 1700707.
- [25] X.F. Liu, T.L. Jin, Z.D. Hood, C.C. Tian, Y.L. Guo, W.C. Zhan, Mechanochemically assisted synthesis of ruthenium clusters embedded in mesoporous carbon for an efficient hydrogen evolution reaction, *ChemElectroChem* 6 (2019) 2719–2725.
- [26] Z.K. Yang, C.M. Zhao, Y.T. Qu, H. Zhou, F.Y. Zhou, J. Wang, Y. Wu, Y.D. Wang, Trifunctional self-supporting cobalt-embedded carbon nanotube films for ORR, OER, and HER triggered by solid diffusion from bulk metal, *Adv. Mater.* 31 (2019) 1808043.
- [27] L. Ye, Y.R. Ying, D.R. Sun, Z.Y. Zhang, L.F. Fei, Z.H. Wen, J.L. Qiao, H.T. Huang, Highly efficient porous carbon electrocatalyst with controllable N-species content for selective CO₂ Reduction, *Angew. Chem. Int. Ed.* 132 (2020) 3270–3277.
- [28] Y. Yu, Z. Peng, M. Asif, H.T.W. Wang, Z.X. Wu, Z.Y. Wang, X.Y. Qiu, H. Tan, H.F. Liu, FeP nanocrystals embedded in N-doped carbon nanosheets for efficient electrocatalytic hydrogen generation over a broad pH range, *ACS Sustain. Chem. Eng.* 6 (2018) 11587–11594.
- [29] Y.K. Zhou, K. Neyerlin, T.S. Olson, S. Pylypenko, J. Bult, H.N. Dinh, T. Gennett, Z.P. Shao, R. O'Hayre, Enhancement of Pt and Pt-alloy fuel cell catalyst activity and durability via nitrogen-modified carbon supports, *Energy Environ. Sci.* 3 (2010) 1437–1446.
- [30] X.J. Zhao, P. Pachfule, S. Li, J.R.J. Simke, J. Schmidt, T. Arne, Bifunctional electrocatalysts for overall water splitting from an iron/nickel-based bimetallic metal-organic framework/dicyandiamide composite, *Angew. Chem. Int. Ed.* 57 (2018) 8921–8926.

- [31] Y.P. Zhang, N. Wang, N. Jia, J. Wang, J. Sun, S. Feng, Z.H. Liu, R.B. Jiang, A low-cost and facile method for the preparation of Fe-N/C-based hybrids with superior catalytic performance toward oxygen reduction Reaction, *Adv. Mater. Interfaces* 6 (2019) 1900273.
- [32] Y. Peng, B.Z. Lu, L.M. Chen, N. Wang, J.E. Lu, Y. Ping, S.W. Chen, Hydrogen evolution reaction catalyzed by ruthenium ion-complexed graphitic carbon nitride nanosheets, *J. Mater. Chem. A* 5 (2017) 18261–18269.
- [33] B.Z. Lu, L. Guo, F. Wu, Y. Peng, J.E. Lu, T.J. Smart, N. Wang, Y.Z. Finck, D. Morris, P. Zhang, N. Li, P. Gao, Y. Ping, S.W. Chen, Ruthenium atomically dispersed in carbon outperforms platinum toward hydrogen evolution in alkaline media, *Nat. Commun.* 10 (2019) 1–11.
- [34] M. Cheng, H.B. Geng, Y. Yang, Y.F. Zhang, C.C. Li, Optimization of the hydrogen-adsorption free energy of Ru-based catalysts towards high-efficiency hydrogen evolution reaction at all pH, *Chem. Eur. J.* 25 (2019) 8579–8584.
- [35] J.W. Su, Y. Yang, G.L. Xia, J.T. Chen, P. Jiang, Q.W. Chen, Ruthenium-cobalt nanoalloys encapsulated in nitrogen-doped graphene as active electrocatalysts for producing hydrogen in alkaline media, *Nat. Commun.* 8 (2017) 1–12.
- [36] S.W. Sun, G.F. Wang, Y. Zhou, F.B. Wang, X.H. Xia, High-performance Ru@C₄N electrocatalyst for hydrogen evolution reaction in both acidic and alkaline solutions, *ACS Appl. Mater. Interfaces* 11 (2019) 19176–19182.
- [37] J. Yu, Y.A. Guo, S.X. She, S.S. Miao, M. Ni, W. Zhou, M.L. Liu, Z.P. Shao, Bigger is surprisingly better: agglomerates of larger RuP nanoparticles outperform benchmark Pt nanocatalysts for the hydrogen evolution reaction, *Adv. Mater.* 30 (2018) 1800047.
- [38] Q. Wang, M. Ming, S. Niu, Y. Zhang, G.Y. Fan, J.S. Hu, Scalable solid-state synthesis of highly dispersed uncapped metal (Rh, Ru, Ir) nanoparticles for efficient hydrogen evolution, *Adv. Energy Mater.* 8 (2018) 1801698.
- [39] K.F. Wang, Q. Chen, Y.Y. Hu, W. Wei, S.Z. Wang, Q. Shen, P. Qu, Crystalline Ru_{0.33}Se nanoparticles-decorated TiO₂ nanotube arrays for enhanced hydrogen evolution reaction, *Small* 14 (2018) 1802132.
- [40] J.T. Cai, T. Chen, L. Cui, Q. Jia, M.S. Liu, R.K. Zheng, G.W. Yan, D. Wei, J.Q. Liu, A three-dimensional and porous bi-nanospheres electrocatalytic system constructed by in situ generation of Ru nanoclusters inside and outside polydopamine nanoparticles for highly efficient hydrogen evolution reaction, *Int. J. Hydrog. Energy* 45 (2020) 6592–6603.
- [41] Y.Z. Li, J. Abbott, Y.C. Sun, J.M. Sun, Y.C. Du, X.J. Han, G. Wu, P. Xu, Ru nanoassembly catalysts for hydrogen evolution and oxidation reactions in electrolytes at various pH values, *Appl. Catal. B: Environ.* 258 (2019) 117952.
- [42] W. Wu, Y. Wu, D. Zheng, K. Wang, Z.H. Tang, Ni@Ru core-shell nanoparticles on flower-like carbon nanosheets for hydrogen evolution reaction at All-pH values, oxygen evolution reaction and overall water splitting in alkaline solution, *Electrochim. Acta* 320 (2019) 134568.
- [43] M.X. Yang, T.L. Feng, Y.X. Chen, J.J. Liu, X.H. Zhao, B. Yang, Synchronously integration of Co, Fe dual-metal doping in Ru@C and CDs for boosted water splitting performances in alkaline media, *Appl. Catal. B: Environ.* 267 (2020) 118657.
- [44] D. Wang, L. Yang, H.B. Liu, D.P. Cao, Polyaniline-coated Ru/Ni(OH)₂ nanosheets for hydrogen evolution reaction over a wide pH range, *J. Catal.* 375 (2019) 249–256.
- [45] P. Jiang, Y. Yang, R.H. Shi, G.L. Xia, J.T. Chen, J.W. Su, Q.W. Chen, Pt-like electrocatalytic behavior of Ru-MoO₂ nanocomposites for the hydrogen evolution reaction, *J. Mater. Chem. A* 5 (2017) 5475–5485.